https://doi.org/10.5194/egusphere-2024-2494
Preprint. Discussion started: 30 August 2024

Accurate Elucidation of Oxidation Under Heavy Ozone Pollution: A Full Suite of Radical Measurement In the Chemical-complex Atmosphere

Renzhi Hu[1], Guoxian Zhang[1,2,×], Haotian Cai[1], Jingyi Guo[1], Keding Lu[4], Xin Li[4], Shengrong Lou[5], Zhaofeng Tan[4], Changjin Hu[1], Pinhua Xie[1,3,××], Wenqing Liu[1,3]

[1] Key Laboratory of Environment Optics and Technology, Anhui Institute of Optics and Fine Mechanics, HFIPS, Chinese Academy of Sciences, Hefei, China

[2] School of Physics and New Energy, Xuzhou University of Technology, Xuzhou, China

[3] College of Resources and Environment, University of Chinese Academy of Science, Beijing, China

[4] State Key Joint Laboratory of Environmental Simulation and Pollution Control, College of Environmental Sciences and Engineering, Peking University, Beijing, China

[5] State Environmental Protection Key Laboratory of the Formation and Prevention of Urban Air Pollution Complex, Shanghai Academy of Environmental Sciences, Shanghai, China

×**Correspondence to:** Guoxian Zhang, School of Physics and New Energy, Xuzhou University of Technology, Xuzhou, China

××**Correspondence to:** Pinhua Xie, Key Laboratory of Environment Optics and Technology, Anhui Institute of Optics and Fine Mechanics, HFIPS, Chinese Academy of Sciences, Hefei, China

Email addresses: gxzhang@aiofm.ac.cn (Guoxian Zhang); phxie@aiofm.ac.cn (Pinhua Xie)

https://doi.org/10.5194/egusphere-2024-2494
Preprint. Discussion started: 30 August 2024

Abstract: The Yangze River Delta (YRD) in China encountered with prolonged ozone pollution in September 2020, which had significant impacts on the respiratory, dermatological, and visual health of local residents. To accurately elucidate the limitations of oxidation processes in the chemical-complex atmosphere, a full suite of radical measurements (OH, HO_2, RO_2, and k_{OH}) was established in YRD region for the first time. The diurnal peaks of radicals exhibited considerable variation due to environmental factors, showing ranges of 3.6 to 27.1×10^6 cm^{-3} for OH, 2.1 to 33.2×10^8 cm^{-3} for HO_2, and 4.9 to 30.5×10^8 cm^{-3} for RO_2. At a heavy ozone pollution episode, the oxidation capacity reached an intensive level compared with other sites, and the simulated OH, HO_2, and RO_2 radicals provided by the RACM2-LIM1 mechanism failed to adequately match the observed data both in concentration and coordinate ratios. Sensitivity tests based on the full suite of radical measurement revealed that the X mechanism accelerated OH regeneration, and the introduction of larger RO_2 isomerization steps alleviated the RO_2-related imbalance by 2 to 4 times. The hypothesis of sensitivity analysis can be chemically validated by the special HCHO contribution to oxidation. Constraining HCHO increased the ChL from 1.94 to 4.45, leading to a 51.54% increase in ozone production during the heavy pollution. The incorporation of complex processes enabled better coordination of HO_2/OH, RO_2/OH, and HO_2/RO_2 ratios comparable to the observed values, and adequately addressed the deficiency in the ozone generation mechanism within a certain range. The full-chain radical detection untangled a gap-bridge between the photochemistry and the intensive oxidation level in the chemical-complex atmosphere, enabling a deeper understanding of the tropospheric radical chemistry at play.

Keywords: FAGE-LIF; Full-chain detection; Radical; P(Ox); HCHO;

https://doi.org/10.5194/egusphere-2024-2494
Preprint. Discussion started: 30 August 2024

1 Introduction

In recent years, China's rapid economic development has led to severe environmental pollution problems, which significant impacted the respiratory, dermatological, and visual health of local residents (Wang et al., 2022c; Huang et al., 2018). This has raised concerns about the coexistence of regional primary and secondary pollution, making air quality improvement efforts a focal point (Liu et al., 2021; Wang et al., 2022a). In the complex atmosphere, near-surface ozone (O_3) is formed through continuous photochemical reactions between nitrogen oxides (NOx ≡ NO+NO_2) and volatile organic compounds (VOCs) under light conditions, while hydroxyl radicals (OH) serve as the main oxidant in the troposphere, converting VOCs into hydroperoxy (HO_2) and organic peroxy (RO_2) radicals (Rohrer et al., 2014; Hofzumahaus et al., 2009). Additionally, the oxidation of nitric oxide (NO) and peroxy radicals produce nitrogen dioxide (NO_2), which is the sole photochemical source of ozone (Lu et al., 2012; Stone et al., 2012).

Despite numerous experimental and theoretical explorations to establish the radical-cored photooxidation mechanism in the troposphere, field observations were primarily focused on HOx (HOx ≡ OH + HO_2) radicals due to the limitations of detection technology (Kanaya et al., 2012; Lu et al., 2012; Hofzumahaus et al., 2009; Yugo Kanaya and Tanimoto, 2007; Ren et al., 2008; Stone et al., 2012; Levy, 1971). Recent advancements in detection technology, such as the application of a new LIF technique (ROxLIF), have made the detection of RO_2 radicals possible (Whalley et al., 2013; Tan et al., 2017a). Moreover, the closure experiment, incorporating field campaigns and box model, has proven to be an effective method for verifying the integrity of radical chemistry at local to global scales (Lu et al., 2019; Tan et al., 2018). Several experiments have indicated that the existing atmospheric chemical mechanism posted challenges in deepening the understanding of the regional pollution explosion (Whalley et al., 2021; Slater et al., 2020; Tan et al., 2017a; Woodward-Massey et al., 2023). For instance, the observation of up to 4×10^9 cm^{-3} of RO_2 radical in the center of Beijing in 2017 (APHH) was significantly underestimated by the MCM v3.3.1 mechanism (Whalley et al., 2021). Further exploring the unreproducible concentration and the oxidation process in the

https://doi.org/10.5194/egusphere-2024-2494
Preprint. Discussion started: 30 August 2024

chemical-complex atmosphere is deemed necessary (Whalley et al., 2021; Woodward-Massey et al., 2023).

The YRD region, situated between the North China Plain (NCP) and Pearl River Delta (PRD), is highly prone to regional transport interactions and aerosol-boundary layer feedback (Jia et al., 2021; Huang et al., 2020). In September 2020, the YRD region experienced a severe episode of secondary pollution, with both the daily maximum 8-hour average ozone (MDA8) and daily average $PM_{2.5}$ concentrations surpassing the pollution threshold, distinguishing it from other megacities (Fig. S1). In an effort to gain a better understanding between the complex radical chemistry and the intensive oxidation level, TROPSTECT-YRD (The experiment on Radical chemistry and Ozone Pollution perSpectively: long-Term Elucidation of the photochemiCal oxidaTion in the Yangze River Delta) was conducted in Hefei during September 2020. Accurate elucidation of the oxidation process under heavy ozone pollution was provided by a full suite of radical measurement (OH, HO_2, RO_2 and k_{OH}) in the chemical-complex atmosphere.

2 Materials and methods

2.1 Site description and instrumentation

The TROPSTECT observation was conducted from 1 to 20 September 2020 at the Science Island background station (31.9° N, 117.2°E) in Hefei, a typical megacity located in the central region of Anhui Province within the Yangtze River Delta. The station is situated on a peninsula with abundant vegetation to the northwest of urban areas and is in close proximity to Dongpu Lake, which is only 200 meters away, and the main road, positioned 250 meters southward (Fig. 1). Consequently, the relatively enclosed environment exhibits typical suburban characteristics of anthropogenic emissions. The station is located in the transition region between urban and suburban areas, reflecting the regional transpor of pollution in Hefei and its surrounding areas.

https://doi.org/10.5194/egusphere-2024-2494
Preprint. Discussion started: 30 August 2024

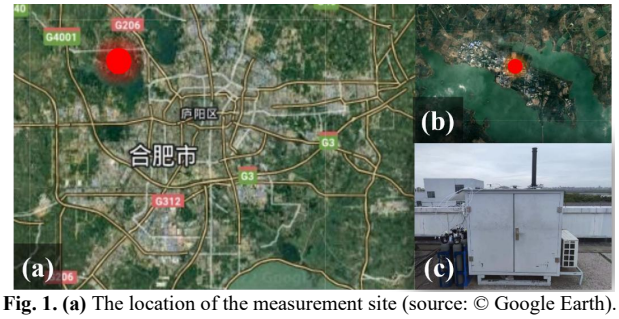

Fig. 1. (a) The location of the measurement site (source: © Google Earth).
(b) The close shot of the measurement site location (source: © Google Earth).
(c) The actual image for the LIF-Box.

Regarding the instrumentation, a group of oxidation-related instruments were installed on the 7th floor of the Comprehensive Building at the Anhui Institute of Optics and Fine Mechanics (AIOFM), with all sampling outlets positioned more than 20 meters above the ground. The details of the instruments measuring various parameters such as meteorological factors (WS, WD, T, RH, P, Jvalues), gas pollutants (O_3, CO, SO_2, NO, NO_2, HONO, HCHO, PAN), and non-methane hydrocarbons (NMHCs) are provided in Table S1.

The measurement of NO, NO_2, O_3, CO, and SO_2 was carried out using commercial Thermo Electron model series instruments. Thereof, NO and NO_2 were measured using a chemical fluorescence method (CL) with an enhanced trace-level NO-NO_2-NOx analyzer (PKU-PL), which achieved a detection limit of 50 ppt (Tan et al., 2017a). The detection of O_3 and SO_2 was conducted through Thermo Electron model 49i and 43i, respectively, while Thermo Electron model 48i was utilized for CO detection. Cavity ring-down spectroscopy (CRDS, Picarro-G2401) was employed for CO detection in parallel, and another ultraviolet absorption instrument (Ecotech EC9810B) was for ozone detection. The instrument inlets were placed within 5 meters of each other for comparison.

To ensure measurement accuracy, the instruments in the campaign underwent zero point calibration procedures during the early (August 31st) and late (September 21st) observation periods, and cross-calibrations for O_3 and CO measurements were carried out during the middle (September 9th). Furthermore, additional zero calibration for Thermo 48i CO detection was undertaken daily from 0:00-0:30 to minimize shift correction. The comparison results revealed high consistency within the instrument accuracy range for both CO and O_3 measurements (Fig. S2(a)(b)).

HONO was detected using a home-built instrument by cavity-enhanced absorption

https://doi.org/10.5194/egusphere-2024-2494
Preprint. Discussion started: 30 August 2024

spectroscopy (CEAS), while formaldehyde was determined by the Hantzsch method (SDL MODEL 4050) (Duan et al., 2018; Yang et al., 2021a). An automated gas chromatograph equipped with a mass spectrometer and flame ionization detector (GC-FID/MS) was employed for the online measurement of 99 VOCs species.

The eight crucial photolysis frequencies ($j(NO_2)$, $j(H_2O_2)$, j(HCHO), j(HONO), $j(NO_2)$, $j(NO_3)$, $j(O^1D)$) were directly measured by a photolysis spectrometer (Metcon, Germany). The unmeasured photolysis frequencies of the remaining active species were computed using Eq.(1):

$$j = l \cdot cos(\chi)^m \cdot e^{-n \cdot sec(\chi)} \quad (1)$$

The variations in photolysis frequency due to solar zenith angle (χ) were adjusted based on the ratio of observed and simulated $j(NO_2)$. The optimal values for parameters (l, m, and n) for different photolysis frequencies were extensively detailed by the MCM v3.3.1 (http://mcm.york.ac.uk/parameters/photolysis_param.htt) (Jenkin et al., 2003; Jenkin et al., 1997).

2.2 Radical measurement

2.2.1 OH, HO_2, RO_2 Concentrations

The laser-induced fluorescence instrument developed by the Anhui Institute of Optics and Fine Mechanics (AIOFM-LIF) was used to simultaneously detect the concentrations of OH, HO_2, and RO_2 radicals, along with OH reactivity (k_{OH}). The OH radical was directly measured by detecting on-resonance fluorescence excited by a 308 nm laser. An indirect measurement for HO_2 was carried out after converting it to OH at a fixed efficiency (Heard and Pilling, 2003).

The laser utilized for fluorescence excitation is a high-frequency tunable dye laser that emits a 308 nm laser, with the laser power divided into a ratio of 0.45:0.45:0.08:0.02. Of this power, 90% is directed towards fluorescence cells for concentration and reactivity detection via optical fibers, respectively. 8% of the laser power is directed to a reference cell, while the remaining 2% is used to monitor real-time power fluctuations. The laser is transmitted through HO_2, OH, and RO_2 cells in turn via a coaxial optical path. Two photodiodes are set up at the end of the reference cell and RO_2 detection cell, respectively. The voltage signals and power fluctuations are compared synchronously to diagnose the laser stability. To maintain detection efficiency, the power inside the measurement cells

https://doi.org/10.5194/egusphere-2024-2494
Preprint. Discussion started: 30 August 2024

should not be less than 10 mW. Sampling nozzles of 0.4 mm are deployed above OH and HO_2 cells for efficient sampling at a flow rate of approximately 1.1 SLM, and the pressure for all fluorescence cells are maintained at 400 Pa. The micro-channel plate (MCP) detects the weak fluorescence signal collected by lens systems with low noise and high gain. Additionally, a digital delay generator (DG645) optimizes the timing control between the laser output, signal detection, and data acquisition. All of these modules are integrated into a sampling box with constant air conditioning, except for the laser.

The detection of RO_2 radicals is more complex compared to the integrated detection of OH and HO_2 radicals (Whalley et al., 2013). To achieve the complete chemical conversion from ROx to HO_2, a crucial role is played by a 66 mm×830 mm aluminium flow tube, whose performance has been confirmed through the CHOOSE-2019 field campaign (Li et al., 2020). A mixture of 0.17% CO and 0.7 ppm NO injected into the flow tube facilitates the reduction of heterogeneous radical loss and enhancement of conversion efficiency. The sampling flow is limited to 7 SLM by a 1 mm nozzle, and the tube pressure is maintained at 25 hPa. In contrast to the HOx cells, the large-diameter nozzle (4 mm) is equipped above the cell, and a high concentration of NO (~300 ppm) facilitates the full magnitude HO_2→OH conversion.

The observation data (H_2O, O_3) is combined with experimental characterization to eliminate ozone photolysis interference, and most interference signals are excluded by utilizing wavelength modulation (Zhang et al., 2022a). A comparison experiment with PKU-LIF demonstrated the consistency of OH measurement in complex atmosphere (Zhang et al., 2022b). For HO_2 measurement, lower NO concentration (~1.6×10^{12} cm^{-3}, corresponding to ~15% conversion efficiency) are selected to limit the RO_2→HO_2 interference to less than 5% (Wang et al., 2021). Since only the total-RO_2 mode is used for the campaign, the additional uncertainty introduced by RO_2/$R(OH)O_2$ classification is negligible (Tan et al., 2017b). The observed maximum daily PAN (11:00-14:00) is only 1.15±0.67 ppb, resulting in a calculated PAN-pyrolytic interference for RO_2 measurement of less than 1 ppt (Fuchs et al., 2008). The general applicability of AIOFM-LIF in complex atmosphere has been demonstrated through various campaigns (Zhang et al., 2022b; Wang et al., 2021; Wang et al., 2019a).

To complete the calibration task, a standard source stably generates equal amounts

https://doi.org/10.5194/egusphere-2024-2494
Preprint. Discussion started: 30 August 2024

of OH and HO_2 radicals (Wang et al., 2020). The radical source is also capable of yielding specific RO_2 by titrating hydrocarbon with OH. It is noteworthy that CH_3O_2 has the highest mixing ratio in the RO_2 species, thus it was chosen to represent for sensitivity calibration. The instrument is calibrated every two days, except during rainy weather. The limit of detection (LOD) for OH, HO_2, and RO_2 in different cells with a typical laser power of 10 mW is measured at 3.3×10^5 cm^{-3}, 1.1×10^6 cm^{-3}, and 2.5×10^6 cm^{-3}, respectively (60 s, 1σ). Measurement accuracy for OH, HO_2, and RO_2 radicals are reported to be 13%, 17%, and 21%, respectively.

2.2.2 OH reactivity(k_{OH})

The detection of k_{OH} in the atmosphere, defined as the reciprocal of OH lifetime, was conducted using a laser flash photolysis laser-induced fluorescence (LP-LIF) instrument (Lou et al., 2010). The configuration structure for k_{OH} measurement has been previously detailed in a study by (Liu et al., 2019). A pulsed laser beam (266 nm with an average power of 15 mJ) is output from a frequency-quadrupled Nd:YAG laser, which generates stable OH radical through flash photolysis in the flow tube. Subsequently, the OH radicals are sampled through a nozzle into a fluorescence cell. The OH fluorescence signal is then detected using laser pump and probe techniques and is fitted to calculate the slope of OH decay (k_{OH}). The detection accuracy, achieved with an integration time of 180 s, is 0.3 s^{-1} (1σ).

2.3 Observation-Based Model

The Regional Atmospheric Chemical Mechanism version 2 (RACM2) incorporating the latest Leuven isoprene mechanism (LIM) was utilized to simulate the concentrations and reactions of OH, HO_2, and RO_2 radicals (Stockwell et al., 1997; Griffith et al., 2013; Peeters et al., 2014). The RACM2-LIM1 mechanism was specifically involved with fewer species compared to the explicit MCM mechanism, thus ensuring higher operational efficiency (Liu et al., 2022). For the base scenario, boundary conditions were established using the observed species listed in Table S1, with assumed concentrations of hydrogen (H_2) and methane (CH_4) at 550 ppb and 1900 ppb, respectively. Moreover, the atmospheric lifetime (τ_D) for all the simulated species was set to 24 hours, and a corresponding first-order loss rate of 1.1 cm/s (assuming a boundary layer height of 1 km). At this lifetime, the simulated ozone concentration closely matched the observed

https://doi.org/10.5194/egusphere-2024-2494
Preprint. Discussion started: 30 August 2024

values (Fig.S3). The time resolution of all constraints was uniformly set to 15 minutes through averaging or linear interpolation. To reinitialize unconstrained species to a steady-state, three days of data were input in advance as the spin-up time.

The local formation of ozone can be accurately quantified through the online measurement of ROx radicals (Tan et al., 2018). To overcome the interference from NO, the total oxidant (Ox), which is defined as the sum of NO_2 and O_3, can serve as a reliable parameter to indicate the level of oxidation. Eq.(2) shows that the rate of NO oxidation by peroxy radicals is equivalent to the production of O_3, denoted as F(Ox):

$$F(O_x) = k_{HO_2+NO}[NO][HO_2] + \sum_i k_{RO_2^i+NO}[NO]RO_2^i \quad (2)$$

The major loss pathways for Ox encompass ozone photolysis, ozonolysis reactions, and radical-related reactions (OH/HO_2+O_3, $OH+NO_2$), represented as D(Ox) in Eq.(3):

$$D(O_x) = \varphi_{OH} j(O^1D)[O_3] + \Sigma i \left\{\varphi_{OH}^i k_{Alkenes+O_3}^i [Alkenes][O_3]\right\} + (k_{O_3+OH}[OH] + k_{O_3+HO_2}[HO_2])[O_3] + k_{OH+NO_2}[OH][NO_2] \quad (3)$$

The net photochemical Ox production rate in the troposphere, denoted as P(Ox) in Eq.(4), can therefore be calculated as the difference between Eqs. (2) and (3):

$$P(O_x) = F(O_x) - D(O_x) \quad (4)$$

Chain Length (ChL) is positively correlated with NO concentration, illustrating the competitive relationship between chain propagation and chain termination reactions (Eq. 5). ChL is defined as the ratio of OH regeneration to the primary source of OH production (Emmerson et al., 2007; Martinez et al., 2003):

$$ChL = \frac{k_{HO_2+NO}[HO_2][NO] + k_{HO_2+O_3}[HO_2][O_3]}{j_{HONO}[HONO] + \phi_{OH} jO^1D[O_3] + \sum(\phi_{OH}^i k^i [alkene]_i [O_3])} \quad (5)$$

3 Results

3.1 Overview of Measurement

During the observation period, the meteorological parameters and trace gas concentrations were plotted in Fig. S4. The timeseries revealed that the peak temperature exceeded 30℃, and the humidity levels remained between 30 – 50% during the daytime. The photolysis rates were observed to peak at noon (11:00 – 13:00), with $j(O^1D)$ and $j(NO_2)$ reaching approximately 3×10^{-5} s^{-1} and 8×10^{-3} s^{-1}, respectively. Brief rainfall events temporarily happened on September 10th, 15th, and 17th, but totally favorable

https://doi.org/10.5194/egusphere-2024-2494
Preprint. Discussion started: 30 August 2024

meteorologies induced the prolonged ozone pollution. The daily maximum 8-hour average ozone concentration (MDA8), as depicted in Fig.2, consistently exceeded the Chinese Grade I national air quality standard (GB3095-2012) throughout the observation, with nine days exceeding the Grade II standard.

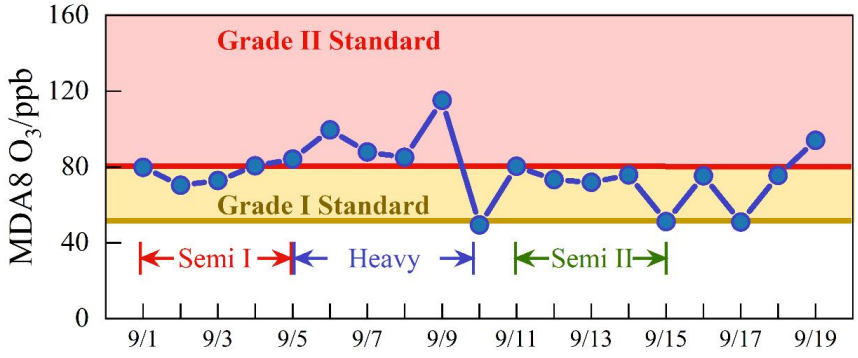

Fig.2. The daily maximum 8 h average O_3 during the campaign. The yellow and red lines denote the Grade I and Grade II national standards for O_3, respectively. Brief rainfall events temporarily happened on10, 15, and 17 Sep.

The ozone pollution can be categorized into three continuous periods based on pollution levels, which disclose transitional 'Semi - Heavy - Semi' pollution characteristics. Fig.3 depicts daily variations in meteorological and trace gas concentrations for different periods. During the Semi I (1 to 5 September) and Semi II (11 to 14 September) periods, the MDA8 levels exceeded Grade I standard, with an average value of 75.92±5.14 ppb and 75.45±3.73 ppb, respectively. Notably, NO levels peaked around 9:00 and rapidly decreased to a few hundred ppt due to photochemistry. In addition, HONO and NO_2 exhibited bimodal variations, with diurnal concentration ranges of 0.09 – 0.50 ppb and 3.35 – 13.77 ppb, respectively. The HONO/NO_2 ratios during both Semi periods were consistent with previous urban/suburban observations, with daytime values of 0.049±0.014 and 0.035±0.012, respectively (Yang et al., 2021b; Shi et al., 2020; Hu et al., 2022). Isoprene levels accumulated during the day and decreased at night during both Semi pollution episodes, with a diurnal average concentration in Semi II only 49.3% of that in Semi I (0.71±0.087 ppb vs 0.35±0.073 ppb). Formaldehyde, as the key oxidation species, exhibited a concentration profile mirroring that of isoprene, with significantly higher concentrations ranging from 1.20 to 36.34 ppb compared to other urban regions (Ma et al., 2022; Yang et al., 2022; Tan et al., 2017b; Yang et al., 2021a). Heavy pollution episodes from 5 to 9 September resulted in daytime ozone concentration

https://doi.org/10.5194/egusphere-2024-2494
Preprint. Discussion started: 30 August 2024

as high as 129.9 ppb, and oxidation-related species such as HCHO, HONO, NOx, and VOCs increased synchronously compared to other days.

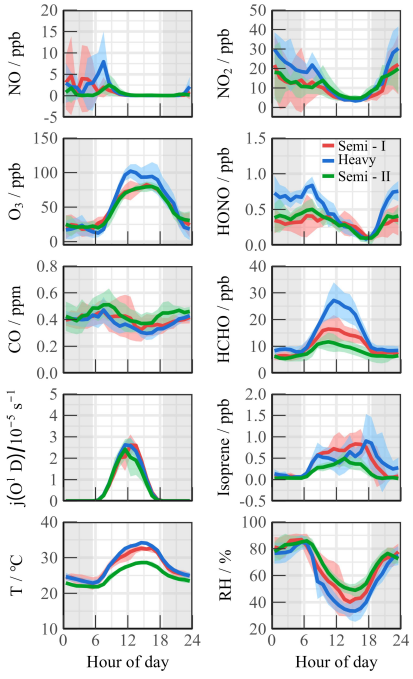

Fig. 3. Mean diurnal profiles of observed meteorological and chemical parameters during the campaign. Three periods were divided for subsequent study (Semi I, Heavy, and Semi II).

3.2 ROx radical concentrations and budgets

The observed and modeled timeseries for OH, HO_2, RO_2, and k_{OH} during the observation time are depicted in Fig.4. The diurnal peaks of radicals exhibited a wide span due to changes in environmental conditions, with ranges of 3.6 – 27.1×10^6 cm^{-3} for OH, 2.1 – 33.2×10^8 cm^{-3} for HO_2, and 4.9 – 30.5×10^8 cm^{-3} for RO_2. Continuous data for k_{OH} observation were acquired within a range of 8.6 – 30.2 s^{-1}. Fig.S5 presents the diurnal profiles of the observed and modeled values during different episodes. The diurnal maximum of OH radical at noon differed between Semi I and Semi II, with 9.28×10^6 cm^{-3} and 5.08×10^6 cm^{-3}, respectively, while total peroxy radicals (HO_2+RO_2) remained at similar levels with 19.43×10^8 cm^{-3} and 18.38×10^8 cm^{-3}. Additionally, the distribution of peroxy radicals are not similar in the two Semi periods, with HO_2/RO_2 ratios of 1.69:1 and 0.76:1, respectively, which reflects the uneven oxidation levels between Semi I and Semi II. During the Heavy ozone pollution, the averaged OH, HO_2, and RO_2

https://doi.org/10.5194/egusphere-2024-2494
Preprint. Discussion started: 30 August 2024

concentrations were 1.90, 2.15, and 1.98 times higher than those in the Semi periods, suggesting a stronger oxidation capacity, with k_{OH} in Heavy being 26.43% and 9.56% higher than in Semi I and Semi II, respectively. Limited anthropogenic emissions in the suburban environment reduced the oxidation contribution by NOx and CO (27.59%). During the heavy pollution, organic species exhibited dominant behavior regarding diurnal reactivity (9.22 s^{-1} for 69.79%), and anthropogenic hydrocarbons were not major k_{OH} sources. With an abundant level (~1 ppb), isoprene contributed more than 10% of the reactivity in the diurnal cycle. Therefore, the effect of BVOCs species (such as monoterpenes, limonene, etc.) on radical chemistry cannot be ignored (Ma et al., 2022; Wang et al., 2022b).

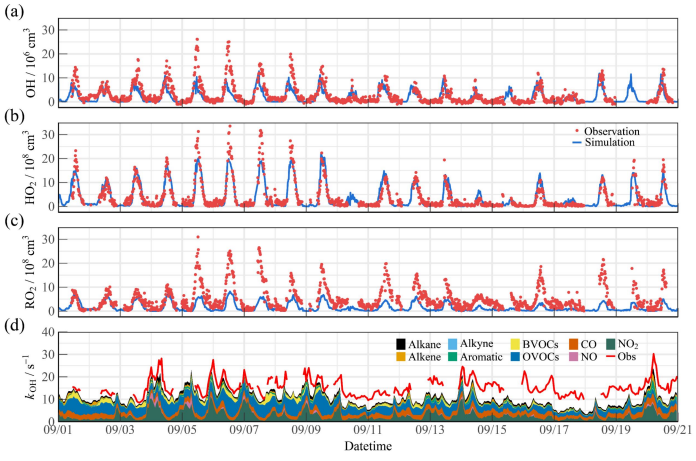

Fig. 4. Timeseries of the observed and modelled parameters for OH, HO_2 and k_{OH} during the observation period. **(a)** OH, **(b)** HO_2, **(c)** k_{OH}.

The significant variations in oxidation can be inferred from the disparities during different pollution periods (Fig.S5). During Semi I, there was a good agreement between the measurement and model for peroxy radicals during the daytime. The RACM2-LIM1 mechanism effectively replicated the morning OH radical concentration. However, following 10:00, NO gradually declined, and the increasing OH concentration could not be accounted for by the HO_2+NO formation channel, resulting in a maximum underestimation of 5.85×10^6 cm^{-3} (Hofzumahaus et al., 2009; Lu et al., 2012). In the Semi II episode, OH was not underestimated in the low-NO regime, with a slight overestimation of HO_2 concentration. However, the simulated RO_2 concentration was only 3.78×10^8 cm^{-3}, whereas observations were 2.77 times larger than the simulation,

https://doi.org/10.5194/egusphere-2024-2494
Preprint. Discussion started: 30 August 2024

indicating the existence of additional reaction pathways that likely propagated the $OH \rightarrow RO_2$ conversion efficiency. A significant discrepancy of radicals existed in the heavy ozone concentration, with OH, HO_2, and RO_2 radicals concurrently underestimated at noon by 8.23×10^6 cm^{-3}, 3.94×10^8 cm^{-3} and 11.59×10^8 cm^{-3}, respectively. The observed HO_2/RO_2 ratio approached 1:1, while the model reflected an unreasonable ratio of 3:1, indicating deficiencies in both primary sources and secondary propagation. Sensitivity tests based on the full suite of radical measurement are performed to explore the missing oxidation properties (Section 4.1).

Fig.5 displays the diurnal profiles of the ROx budget during different episodes. In Semi I, formaldehyde photolysis showed a higher contribution (38.6%), while HONO photolysis (21.0%) and ozone photolysis (24.7%) accounted for similar proportions in primary sources. The contribution of photolysis from other OVOCs was comparable to that of ozonolysis reactions (7.2% vs. 4.8%). However, in Semi II, the decreased oxidation level was attributed to lower ROx sources, despite the similar proportions. During the Heavy period, the primary sources dramatically increased (up to ~10 ppb/h), with HCHO photolysis contributing the most, alongside other sources at common levels (ranging between 1.74 – 2.66 ppb/h) in the YRD region (Ma et al., 2022). Fast HCHO oxidation dominated the radical primary source during heavy ozone pollution, which contrasts with the dominant role of $HONO/O_3$ in other megacities (Yang et al., 2022; Tan et al., 2017b; Yang et al., 2021a).

The radical removal rate during the daytime was generally balanced with production contributions. In the morning, owing to high NOx concentrations, radical termination was mainly dominated by $OH+NO_2$, OH+NO, RO_2+NO, and RO_2+NO_2. Furthermore, the formation of peroxy nitrate accounted for a certain proportion (~5%). As NOx concentrations decreased after 10:00, self-reactions in peroxy radicals became significant.

https://doi.org/10.5194/egusphere-2024-2494
Preprint. Discussion started: 30 August 2024

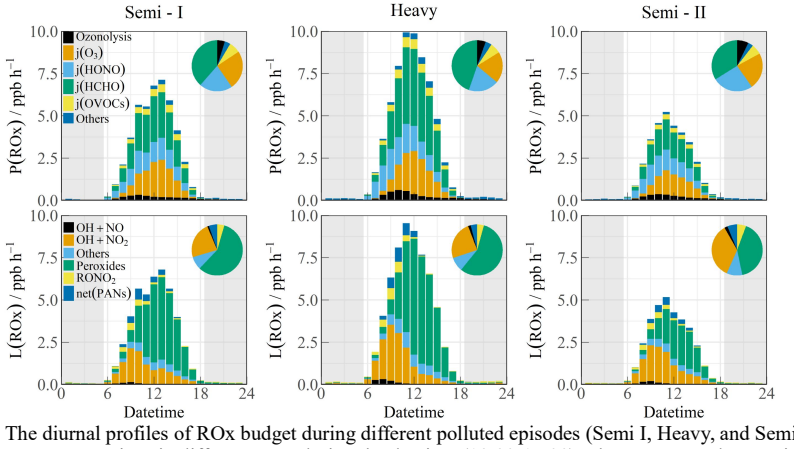

Fig. 5. The diurnal profiles of ROx budget during different polluted episodes (Semi I, Heavy, and Semi II). The pie chart denotes proportions in different parts during the daytime (10:00-15:00). The grey areas denote nighttime.

3.3 Oxidation comparison

The concentration of OH radicals during the daytime is a crucial indicator of atmospheric oxidation levels (Liu et al., 2021). Table 1 summarized radicals and related parameters for regions with similar latitudes (32.0° ± 2° N, $j(O^1D) \approx 2.5 \pm 0.5\times10^{-5}$ s^{-1}). The joint influence of solar radiation and local photochemistry resulted in megacities exhibiting intense oxidation levels in summer/autumn, characterized by OH radicals being maintained at approximately 10.0×10^6 cm^{-3} at noon. Notably, an observation in Houston revealed an OH concentration of nearly 20.0×10^6 cm^{-3}, with k_{OH} of 10 s^{-1} (Mao et al., 2010). In areas such as Los Angeles, Pasadena, and Tokyo, the propagation efficiency of radicals was restricted due to fresh anthropogenic emissions. OH concentrations were only half of those observed in other megacities, with higher inorganic-dominated k_{OH} recorded (Pasadena, ~20 s^{-1}) (George et al., 1999; Griffith et al., 2016; Yugo Kanaya et al., 2007). In the TROPSTECT observation, the observed k_{OH} exceeded the mean value at the same latitude (>15 s^{-1}). Additionally, during the Heavy episode, higher OH concentration (13.5×10^6 cm^{-3}) was found, comparable to the highest level at regions with similar latitude (Houston 2000/2006, (Mao et al., 2010)). Synchronous elevation in radical concentration and reactivity indicated a strong oxidation level in the YRD region.

The observations in the YRD region showed a stable conversion factor (OH-$j(O^1D)$) of $4\pm1 \times 10^{11}$ cm^{-3} s, which was comparable to other megacities in the PRD, NCP, and SCB regions (Ma et al., 2022; Tan et al., 2019). The corresponding slope between OH

https://doi.org/10.5194/egusphere-2024-2494
Preprint. Discussion started: 30 August 2024

concentration and solar radiation was used to quantify the oxidation efficiency from photolysis, and it was observed that a higher slope of 5.3×10^{11} cm^{-3} s during the Heavy period indicated an active radical chemistry. This implies that there is a strong oxidation efficiency from photolysis in the YRD region.

During summer and autumn seasons, photochemical pollution is a common occurrence, as noted by (Tan et al., 2021). Analysis of radical concentration across different regions reveals that the YRD region exhibited concentrations higher than 10^7 cm^{-3}, slightly lower than in Guangzhou in 2006 but consistent with observations in other megacities (Ma et al., 2022; Tan et al., 2017a; Lu et al., 2012; Yang et al., 2021a). Conversely, winter is characterized by haze pollution (Ma et al., 2019). An urban site in Shanghai reported a peak OH concentration of 2.6×10^6 cm^{-3}, closely resembling the 1.7 – 3.1×10^6 cm^{-3} range found in polluted winter atmospheres (Zhang et al., 2022a). Although no significant regional disparities in oxidation levels were detected in agglomerations, attention should be directed to the YRD region due to its elevated radical concentration, reactivity, and photolysis efficiency, signaling the need to investigate its role in radical chemistry.

Table 1. Summary of radical concentrations and related species concentrations at regions with similar latitude and megapolitan areas in China. All data are listed as the average in noontime (11:00~13:00).

Location	Latitude	Year	OH (10^6 cm^{-3})	k_{OH} (s^{-1})	j(O^1D) (10^{-5} s^{-1})	Slope (10^{11} cm^{-3} s)	X (ppb)	References
Regions with similar latitude								
Los Angeles	34.1° N	Sep 1993	6.0	-	-	-	-	(George et al., 1999)
Nashville	36.2° N	Jun–Jul 1999	10.0	10.2	3.0	3.3[c]	-	(Martinez et al., 2003)
Houston	29.7° N	Aug 2000	20.0	9.0[b]	3.0	6.7[c]	-	(Mao et al., 2010)
Tokyo	35.6° N	Jul–Aug 2004	6.3	-	2.5	3.0	-	(Yugo Kanaya et al., 2007)
Houston	29.7° N	Sep 2006	15.0	11.0	3.1	5.0[c]	-	(Mao et al., 2010)
Pasadena	34.1° N	May-Jun 2010	4.0	20.0	2.5	1.6[c]	-	(Griffith et al., 2016)
Taizhou	32.6° N	May-Jun 2018	10.6	10.8[a]	2.1	4.8	0.10	(Ma et al., 2022)
Chengdu	30.7° N	Aug 2019	10.0	8.0	2.2	4.1	0.25	(Yang et al., 2021a)
TROPSTECT (Heavy)	31.9° N	Sep 2020	13.5	16.0	2.6	5.3	0.50	This work
TROPSTECT (Semi)	31.9° N	Sep 2020	7.2	14.2	2.4	3.1	0.25	This work
Regions in megapolitan areas in China								
Guangzhou (PRD)	23.5° N	Jul 2006	12.6	17.9	3.5[b]	4.5	0.85	(Lu et al., 2012)
Wangdu (NCP)	38.7° N	Jun–Jul 2014	8.3	15.0	1.8	4.5	0.10	(Tan et al., 2017b)
Beijing (NCP)	39.9° N	May–Jun 2017	9.0	30.0	2.4	3.8[c]	~0	(Whalley et al., 2021)
Taizhou (YRD)	32.6° N	May-Jun 2018	10.6	10.8[a]	2.1	4.8	0.10	(Ma et al., 2022)
Shenzhen (PRD)	22.6° N	Sep-Oct 2018	4.5	21.0	1.8	2.4	0.10	(Yang et al., 2022)

https://doi.org/10.5194/egusphere-2024-2494
Preprint. Discussion started: 30 August 2024

Chengdu (SCB)	30.7° N	Aug 2019	9.0	8.0	2.2	4.0	0.25	(Yang et al., 2021a)
Hefei (YRD)	31.9° N	Sep 2020	10.4	14.3	2.4	4.4	0.30	This work

[a] The modeled k_{OH}.
[b] Value only in the afternoon.
[c] Using the ratio of OH / $j(O^1D)$

4 Discussion

4.1 Measurement–model reconciliation for radicals

4.1.1 OH underestimation

Full suite of OH, HO_2, RO_2 and k_{OH} was utilized in the TROPSTECT campaign to untangle a thorough understanding of oxidation mechanisms where base model failed. One specific phenomenon was the absence of an OH source in situations where NO levels gradually decreased after 10:00. A sensitivity test was conducted introducing a species X, analogous to NO, to enhance OH regeneration (Fig. 6, $RO_2 \rightarrow HO_2$ and $HO_2 \rightarrow OH$) (Hofzumahaus et al., 2009). It was found that the addition of as little as 0.25 ppb X was sufficient to compensate for the full magnitude of the OH underestimation in the low NO region (Fig. 6). The employment of the X mechanism not only accelerated OH regeneration but also augmented the removal channel of peroxy radicals, which consequently led to a reduction in both HO_2 and RO_2 radical concentrations compared to the base scenario.

The underdetermined radical sources in China were corrseponding to the oxidation level (Ma et al., 2022; Tan et al., 2017a; Lu et al., 2012; Yang et al., 2021a; Wang et al., 2019b). The required X level typically ranged from 0.1 to 0.3 ppb, with the exception of the Backgarden observation which required 0.85 ppb X, as indicated in Table 1 (Lu et al., 2012). A minimum limit of 0.1 ppb X was established to account for any missing reactivity (Ma et al., 2022). Notably, throughout the entire observation, a strong agreement between the modeled and observed OH was achieved when a mixture of 0.25 ppb X was incorporated into the base scenario, consistent with the the order of magnitude in Chengdu (Yang et al., 2021a). During the Heavy period, the augmented photochemistry resulted in complex oxidation, necessitating an additional missing OH source equivalent to 0.5 ppb X to fully address the underestimation of OH.

https://doi.org/10.5194/egusphere-2024-2494
Preprint. Discussion started: 30 August 2024

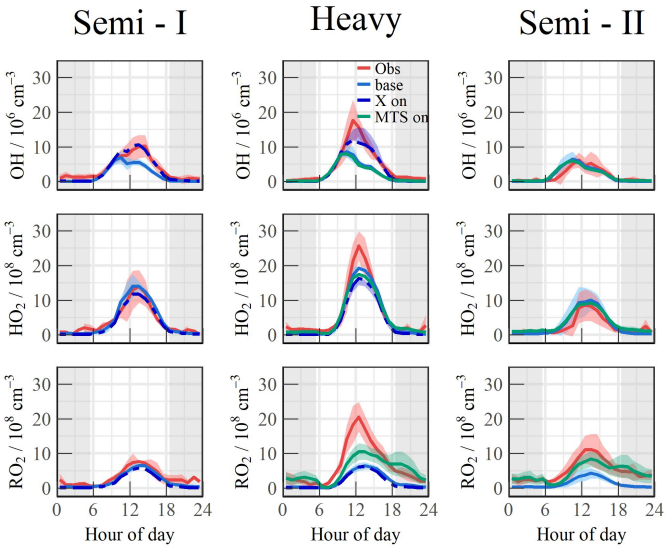

Fig. 6. The mean diurnal profiles of measured and modeled OH, HO_2 and RO_2 concentrations at different scenarios. Sensitivity tests included three scenarios (Scenario 1: base case; Scenario 2: X mechanism on. The dashed line represented the performance of 0.25 ppb X introduced in the Semi I and Heavy episodes, and the blue shadow denoted the upper limit for X influence (0.5 ppb); Scenario 3: monoterpene mechanism on; Both API and LIM were added into the base model as upper and lower limits for the influence of monoterpenes, and the mean of the two values was taken as the average effect. The grey areas denote nighttime.

4.1.2 RO_2 underestimation

The base scenario in Semi II is capable of accurately reproducing the concentrations of OH and HO_2 radicals within the data uncertainty. However, the simulated RO_2 concentration by the base model is only 3.78×10^8 cm^{-3}, which does not align with the observed oxidation levels in YRD, indicating a clear discrepancy. This underestimation is similarly evident in the APHH observation in Beijing, as the highest observed concentration of RO_2 radicals reached 5.5×10^9 cm^{-3}, far exceeding the level predicted by the MCM v3.3.1 mechanism (Whalley et al., 2021). The failure to reproduce the RO_2 concentration reflects the inadequacy of the mechanisms related to RO_2 radicals due to diverse oxidation reactions. This issue is further elucidated by previous studies, which highlighted the possibility of certain VOCs undergoing more intricate isomerization or fragmentation steps to sustain the long lifetime of RO_2 radicals (Whalley et al., 2018; Whalley et al., 2021).

The union of k_{OH} and RO_2 measurement can help reveal the magnitude of missing RO_2 as a hypothesis of sensitivity analysis. During the Semi II period, discrepancy of OH reactivity (~3 – 5 s^{-1}) between measurement and model suggested that an additional driving force was necessary to complete the OH to RO_2 step. The derivative of α-Pinene,

https://doi.org/10.5194/egusphere-2024-2494
Preprint. Discussion started: 30 August 2024

$C_{96}O_2$, could undergo four $RO_2 \rightarrow RO_2$ propagations before termination, thereby making it a plausible source of the underestimation of RO_2 (Whalley et al., 2021). In the EXPLORE-2018 campaign in the YRD region, the diurnal average of monoterpenes peaked at 0.55 ppb between 11:00 and 13:00, with an oxidation efficiency of approximately 1.5 ppb/h (Wang et al., 2022b). To compensate for the missing k_{OH} within a reasonable range, approximately 0.4 ppb of monoterpene was introduced into the base scenario. The RACM2 mechanism identified α-pinene (API) and limonene (LIM) as representative monoterpenes species. Sensitivity tests were conducted by incorporating API and LIM into models as upper and lower limits for the influence of monoterpenes, with reaction rates of 5.3×10^{-11} cm^{-3} s^{-1} and 1.6×10^{-10} cm^{-3} s^{-1} at 298 K, respectively (Ma et al., 2022). The mean of these values was considered the average effect of monoterpenes chemistry, and depicted as the green line in Fig.6. In the 'MTS on' scenario, the chemistry of peroxy radicals in Semi II was reasonably described by decreasing the obs-to-mod ratio of peroxy radicals from 2.2 to 1.3. Furthermore, the introduction of additional RO_2 isomerization steps had minimal impact on HOx chemistry, with changes in daytime OH and HO_2 concentrations of less than 5×10^5 cm^{-3} and 2.5×10^7 cm^{-3}, respectively. This demonstrates the robustness of HOx radical in response to potential monoterpene.

During the heavy ozone pollution, a more pronounced level of oxidation was observed, as evidenced by the diurnal peak radical concentrations being 2.58, 1.22, and 3.02 times higher than the simulated values for OH, HO_2 and RO_2, respectively. Incorporating monoterpenes into the base model led to a substantial 1.93-fold increase in the modeled RO_2. However, the model was unable to reproduce over half of the concentration due to unidentified oxidation processes, as illustrated in Fig. 7. Previous researches highlighted the significance of investigating whether the sink pathways accurately reflect conditions in the actual atmosphere (Tan et al., 2017a; Woodward-Massey et al., 2023). In regions with low NOx levels, peroxy radical removal is primarily achieved through self-reaction. Manipulating the self-reaction rate of peroxy radicals by approximately five-fold, and the extended lifetime counterbalance their supplementary consumption by non-traditional regeneration mechanisms. Consequently, the concentrations of OH, HO_2, and RO_2 radicals increased simultaneously, and the

https://doi.org/10.5194/egusphere-2024-2494
Preprint. Discussion started: 30 August 2024

obs-to-mod ratio of daytime RO_2 shifted from 3.02 to 1.37.

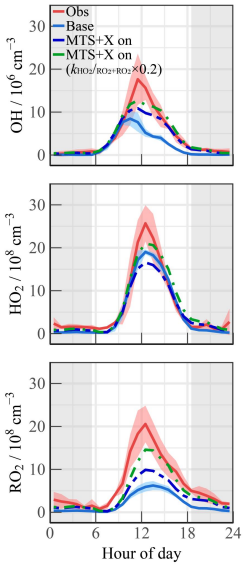

Fig. 7. The mean diurnal profiles of measured and modeled OH, HO_2 and RO_2 concentrations in the Heavy period. The dashed blue line indicates the scenario synchronously considering monoterpene chemistry and non-traditional regeneration mechanisms (MTS+X). The dashed green line represents artificially reducing the rate of peroxy radical self-reaction (about 5 times) on top of the MTS+X scenario.

4.1.3 P(Ox) underestimation

Upon completing the hypothetical investigation into the radical underestimation, a sensitivity comparison between observed and modelled P(Ox) was conducted across the entire range of NO concentrations, as depicted in Fig. 8(a)(b). With increasing NO concentration, the overall P(Ox) amplified, reaching a maximum of approximately 30 ppb/h. This variation has been validated through multiple observations in Wangdu, APHH, and other studies (Tan et al., 2017b; Whalley et al., 2021; Whalley et al., 2018). However, the imperfect understanding of the mechanisms related to peroxy radicals ultimately leads to misjudgment of the ozone production process in high NO regimes, with a degree of underestimation close to 10 times, as illustrated in Fig. 8(b).

https://doi.org/10.5194/egusphere-2024-2494
Preprint. Discussion started: 30 August 2024

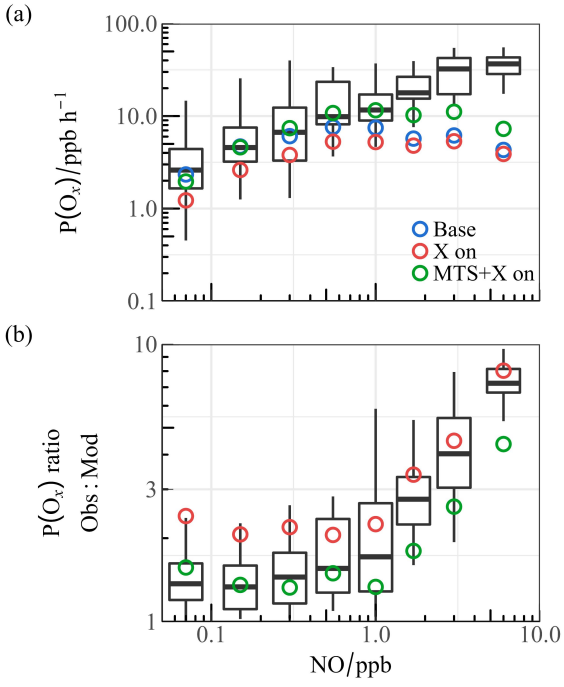

Fig. 8. The relationship between NO and **(a)** P(Ox), **(b)** P(Ox) (Obs:Mod). Boxplot diagrams are used to illustrate the minimum, 25th percentile, median, 75th percentile, and maximum values of the observed dataset. The circles represent the median values for the base model as well as for different mechanisms added to the model within various ranges.

Although the inclusion of the X mechanism improves the agreement between simulated and observed OH concentrations in the low-NO range, it has a negative effect on the P(Ox) simulation. The introduction of a major source of RO_2 can help address the underestimation problem in the base scenario, as the lack of RO_2 species and related reaction rates is an important factor leading to deviations in the simulation of ozone production rates (Tan et al., 2017a). The combination of the X mechanism and monoterpene chemistry is shown to better harmonize the relationship between HO_2 and RO_2. Notably, the deficiency in the ozone generation mechanism was adequately explained within a certain range in the 'MTS+X On' scenario, leading to an enhancement in the simulation performance of P(Ox) in the high NOx region (Fig. 8(b)). Therefore, reasonable simulation of the concentration of peroxy radicals is key to accurately quantifying the process of ozone generation.

4.2 Effect of mechanism reconciliation on oxidation

Both radical concentration and oxidation coordinating deficiency are worthy of

https://doi.org/10.5194/egusphere-2024-2494
Preprint. Discussion started: 30 August 2024

examine (Fig. S6). To eliminate the influence of non-photolytic processes, only the daytime concentration range with $j(O^1D)$ greater than 5×10^{-6} s^{-1} was selected. The boxplots illustrate the ratio of observation to simulation (base model), with the circles representing the average values after integrating different mechanisms into the base scenario. In the low NO regime (NO < 1 ppb), the OH underestimation was consistently prominent as NO concentration decreased, and the base model was able to reasonably reflect the HO_2 distribution contrastly. As NO levels increased, the simulated OH concentration aligned well with the observation, but both HO_2 and RO_2 concentrations exhibited underprediction. RO_2 underestimation extended across the entire NO range, and could rise to over 10 times when NO levels reached about 10 ppb. Sensitivity tests based on the full suite of radical measurement revealed that the X mechanism accelerated OH regeneration, and the introduction of larger RO_2 isomerization steps alleviated the absence of certain sources by 2 to 4 times.

The coordinate ratios of radical serves as another test for ROx propagation (Fig. 9). The observed HO_2/OH ratio is approximately 100, declining to some extent as the concentration of NO increases, which is consistent with previous studies (Griffith et al., 2016; Griffith et al., 2013). However, the base model does not accurately replicate the curve depicting the change in HO_2/OH ratio, as shown in Fig. 9 (a). At low NO levels, the ratio significantly overestimated and shows a steeper decline compared to the base scenario as NO levels increase. Furthermore, the observed RO_2/OH ratios remain around 100, whereas the predicted values are significantly underestimated when NO exceeds 1 ppb (refer to Fig. 9(b)). In terms of the observed HO_2/RO_2 ratio, it maintains a relatively constant trend within the range of 0.5 – 1.5, while the model overestimated by more than twice, highlighting an inconsistency between the conversion of $RO_2 \rightarrow HO_2$. The incorporation of the X mechanism has proven to be effective in a balanced HO_2/OH ratio as illustrated in Fig.9(a), but amplifing the termination pathway for HO_2 and RO_2, which altered the coordination between RO_2 and OH across the entire NO range (Fig. 9(b)). The connection between unconditional OH source and larger RO_2 isomerization in chemically complex environments is key to fully understanding tropospheric chemistry, and a better coordination of HO_2/OH, RO_2/OH, and HO_2/RO_2 ratios are established by incorporating additional mechanisms.

https://doi.org/10.5194/egusphere-2024-2494
Preprint. Discussion started: 30 August 2024

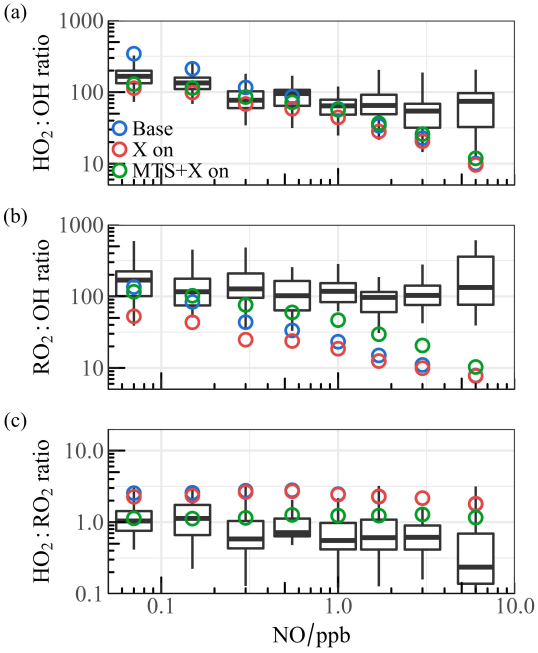

Fig. 9. The ratios for **(a)** HO_2/OH, **(b)** RO_2/OH, and **(c)** HO_2/RO_2 show a correlation with NO levels. Boxplot diagrams are used to illustrate the minimum, 25th percentile, median, 75th percentile, and maximum values of the observed dataset. The circles represent the median values for the base model as well as for different mechanisms added to the model within various ranges.

4.3 Special HCHO contribution accelerate ozone production

Amplification of radical cycling can be distinguished by the OVOCs photochemical contribution (Qu et al., 2021). The special formaldehyde distribution was discovered during severe ozone pollution, with the average value of 21.81±4.57 ppb (11:00 – 13:00), emboding the fast oxidation feedback to accelerate ozone production. The distribution ratio between peroxy radicals shows that the observed HO_2/RO_2 remains stable around ~1, whereas the simulated values exhibit a strong positive correlation with photochemistry, ranging between 2-4 (Fig.10). When formaldehyde is unconstrained, the simulated HO_2/RO_2 contraryly aligned with observations, indicating that the photochemistry efficiencies of formaldehyde and other OVOCs is comparable under the current chemical mechanism. Since formaldehyde is a source of HO_2 radicals but does not directly produce RO_2 radicals, constraining formaldehyde can partially compensate for the HO_2 radical cycle, thereby enhancing the accuracy of HOx radical chemistry research. However, the base model underestimates the OVOCs feedback to RO_2 radicals during the heavy pollution. The introduction of larger RO_2 isomerization steps (possibly caused by OVOCs,

https://doi.org/10.5194/egusphere-2024-2494
Preprint. Discussion started: 30 August 2024

monoterpenes) kept both the HO_2/RO_2 ratio and the P(Ox) comparable to observed results in the MTS+X scenario during different pollution periods, which chemically validated the hypothesis of the sensitivity analysis (Section 4.2&Fig.S7).

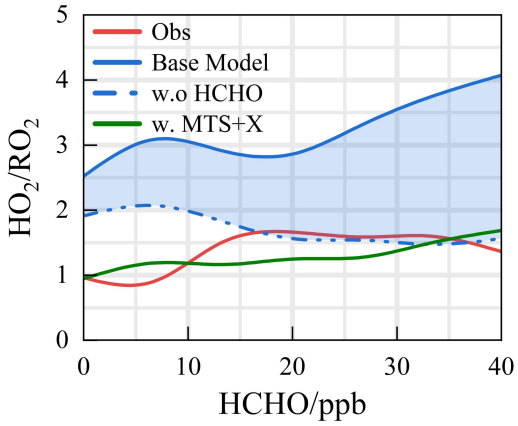

Fig. 10. The ratios for HO_2/RO_2 show a correlation with HCHO levels. The blue shading represents the range of variation from constrained to unconstrained formaldehyde conditions.

The relationship between radical cycling and ozone pollution is established through chain length (ChL) and ozone production rate (P(Ox)) (Fig.S8). Overall, the average chain length during different periods ranges from 1.4 to 6.1, similar to results from multiple photochemical pollution seasons (Yang et al., 2021a; Martinez et al., 2003; Shirley et al., 2006). To evaluate the impact of high formaldehyde concentrations on severe pollution formation, the peak chain length decreased by 38.22%, 55.91%, and 39.15% after removing formaldehyde constraints from the base model. P(Ox) and ChL exhibit overall temporal consistency. Constraining formaldehyde increased the peak radical cycling rate from 1.94 to 4.45 during heavy pollution periods, and the rapid radical cycling accelerates secondary pollution formation, with peak ozone production rates increasing by 51.54%. With the implementation of full-chain radical detection, additional measurements targeting more OVOCs should also be conducted to untangle the RO_2-related imbalance, and then accurately elucidating the oxidation under severe ozone pollution.

5 Conclusion

The full suite radical measurement of OH, HO_2, RO_2 and k_{OH} was first deployed in the YRD region (TROPSTECT) and encountered with a prolonged ozone pollution in

https://doi.org/10.5194/egusphere-2024-2494
Preprint. Discussion started: 30 August 2024

September 2020. The diurnal peaks of radicals exhibited considerable variation due to environmental factors, showing ranges of 3.6 to 27.1×10^6 cm^{-3} for OH, 2.1 to 33.2×10^8 cm^{-3} for HO_2, and 4.9 to 30.5×10^8 cm^{-3} for RO_2. Continuous k_{OH} data fell within a range of 8.6 – 30.2 s^{-1}, demonstrating the dominant behavior of organic species in diurnal reactivity. Furthermore, observations in the YRD region were found to be similar to those in other megacities, suggesting no significant regional differences in oxidation levels were observed in agglomerations overall.

At a heavy ozone pollution episode, the oxidation level reached intensive compared with other sites, and the simulated OH, HO_2, and RO_2 radicals provided by the RACM2-LIM1 mechanism failed to adequately match the observed data both in radical concentration and coordinate ratios. Sensitivity tests based on the full suite of radical measurement revealed that the X mechanism accelerated OH regeneration, and the introduction of larger RO_2 isomerization steps alleviated the RO_2-related imbalance. The incorporation of complex processes enabled better coordination of HO_2/OH, RO_2/OH, and HO_2/RO_2 ratios, and adequately addressed the deficiency in the ozone generation mechanism within a certain range. The hypothesis of sensitivity analysis can be chemically validated by the special HCHO contribution to oxidation. Constraining HCHO increased the ChL from 1.94 to 4.45, leading to a 51.54% increase in ozone production during the heavy pollution. This study enabled a deeper understanding of the tropospheric radical chemistry at play. Notably,

- ✓ A full suite of radical measurement can untangle the gap-bridge for the base model in more chemically-complex environments as an hypothesis of sensitivity tests.
- ✓ Additional measurements targeting more OVOCs should also be conducted to fulfill the RO_2-related imbalance, and then accurately elucidating the oxidation under severe ozone pollution.

https://doi.org/10.5194/egusphere-2024-2494
Preprint. Discussion started: 30 August 2024

Financial support

This work was supported by the National Key R&D Program of China (2022YFC3700301), the National Natural Science Foundation of China (62275250, U19A2044, 42030609), the Natural Science Foundation of Anhui Province (No. 2008085J20), the Anhui Provincial Key R&D Program (2022l07020022), and the Distinguished Program of Jianghuai Talents Program of Excellence (HYRCSTZ202401).

Data availability

The data used in this study are available upon request (rzhu@aiofm.ac.cn).

Author contributions

WQ Liu, PH Xie, RZ Hu contributed to the conception of this study. RZ Hu and GX Zhang performed the data analyses and manuscript writing. All authors contributed to measurements, discussed results, and commented on the paper.

Competing interests

The contact author has declared that none of the authors has any competing interests.

https://doi.org/10.5194/egusphere-2024-2494
Preprint. Discussion started: 30 August 2024

References

Duan, J., Qin, M., Ouyang, B., Fang, W., Li, X., Lu, K., Tang, K., Liang, S., Meng, F., Hu, Z., Xie, P., Liu, W., and Häsler, R.: Development of an incoherent broadband cavity-enhanced absorption spectrometer for in situ measurements of HONO and NO_2, Atmos Meas Tech, 11, 4531-4543, 10.5194/amt-11-4531-2018, 2018.

Emmerson, K. M., Carslaw, N., Carslaw, D. C., Lee, J. D., McFiggans, G., Bloss, W. J., Gravestock, T., Heard, D. E., Hopkins, J., Ingham, T., Pilling, M. J., Smith, S. C., Jacob, M., and Monks, P. S.: Free radical modelling studies during the UK TORCH Campaign in Summer 2003, Atmos Chem Phys, 7, 167-181, 10.5194/acp-7-167-2007, 2007.

Fuchs, H., Holland, F., and Hofzumahaus, A.: Measurement of tropospheric RO_2 and HO_2 radicals by a laser-induced fluorescence instrument, Rev of Sci Inst, 79, 084104, 10.1063/1.2968712, 2008.

George, L. A., Hard, T. M., and O'Brien, R. J.: Measurement of free radicals OH and HO_2 in Los Angeles smog, J Geophys Res-Atmos, 104, 11643-11655, 1999.

Griffith, S. M., Hansen, R. F., Dusanter, S., Stevens, P. S., Alaghmand, M., Bertman, S. B., Carroll, M. A., Erickson, M., Galloway, M., Grossberg, N., Hottle, J., Hou, J., Jobson, B. T., Kammrath, A., Keutsch, F. N., Lefer, B. L., Mielke, L. H., O'Brien, A., Shepson, P. B., Thurlow, M., Wallace, W., Zhang, N., and Zhou, X. L.: OH and HO_2 radical chemistry during PROPHET 2008 and CABINEX 2009-Part 1: Measurements and model comparison, Atmos Chem Phys, 13, 5403-5423, 10.5194/acp-13-5403-2013, 2013.

Griffith, S. M., Hansen, R. F., Dusanter, S., Michoud, V., Gilman, J. B., Kuster, W. C., Veres, P. R., Graus, M., de Gouw, J. A., Roberts, J., Young, C., Washenfelder, R., Brown, S. S., Thalman, R., Waxman, E., Volkamer, R., Tsai, C., Stutz, J., Flynn, J. H., Grossberg, N., Lefer, B., Alvarez, S. L., Rappenglueck, B., Mielke, L. H., Osthoff, H. D., and Stevens, P. S.: Measurements of hydroxyl and hydroperoxy radicals during CalNex-LA: Model comparisons and radical budgets, J Geophys Res-Atmos, 121, 4211-4232, 10.1002/2015jd024358, 2016.

Heard, D. E. and Pilling, M. J.: Measurement of OH and HO_2 in the troposphere, Chemical reviews, 103, 5163-5198, 10.1021/cr020522s, 2003.

Hofzumahaus, A., Rohrer, F., Lu, K., Bohn, B., Brauers, T., Chang, C.-C., Fuchs, H., Holland, F., Kita, K., Kondo, Y., Li, X., Lou, S., Shao, M., Zeng, L., Wahner, A., and Zhang, Y.: Amplified Trace Gas Removal in the Troposphere, Science, 324, 1702-1704, 10.1126/science.1164566, 2009.

Hu, B., Duan, J., Hong, Y., Xu, L., Li, M., Bian, Y., Qin, M., Fang, W., Xie, P., and Chen, J.: Exploration of the atmospheric chemistry of nitrous acid in a coastal city of southeastern China: results from measurements across four seasons, Atmos Chem Phys, 22, 371-393, 10.5194/acp-22-371-2022, 2022.

Huang, J., Pan, X., Guo, X., and Li, G.: Health impact of China's Air Pollution Prevention and Control Action Plan: an analysis of national air quality monitoring and mortality data, Lancet Planet Health, 2, e313-e323, 10.1016/S2542-5196(18)30141-4, 2018.

Huang, X., Ding, A., Wang, Z., Ding, K., Gao, J., Chai, F., and Fu, C.: Amplified transboundary transport of haze by aerosol–boundary layer interaction in China, Nature Geoscience, 13, 428-434, 10.1038/s41561-020-0583-4, 2020.

Jenkin, M. E., Saunders, S. M., and Pilling, M. J.: The tropospheric degradation of volatile organic compounds: A protocol for mechanism development, Atmos Environ, 31, 81-104, 10.1016/s1352-2310(96)00105-7, 1997.

Jenkin, M. E., Saunders, S. M., Wagner, V., and Pilling, M. J.: Protocol for the development of the Master Chemical Mechanism, MCM v3 (Part B): tropospheric degradation of aromatic volatile organic compounds, Atmos Chem Phys, 3, 181-193, 10.5194/acp-3-181-2003, 2003.

Jia, W., Zhang, X., and Wang, Y.: Assessing the pollutant evolution mechanisms of heavy pollution episodes in the Yangtze-Huaihe valley: A multiscale perspective, Atmos Environ, 244, 10.1016/j.atmosenv.2020.117986, 2021.

Kanaya, Y., Hofzumahaus, A., Dorn, H. P., Brauers, T., Fuchs, H., Holland, F., Rohrer, F., Bohn, B., Tillmann, R., Wegener, R., Wahner, A., Kajii, Y., Miyamoto, K., Nishida, S., Watanabe, K., Yoshino, A., Kubistin, D., Martinez, M., Rudolf, M., Harder, H., Berresheim, H., Elste, T., Plass-Duelmer, C., Stange, G., Kleffmann, J., Elshorbany, Y., and Schurath, U.: Comparisons of observed and modeled OH and HO_2 concentrations during the ambient measurement period of the HO(x)Comp field campaign, Atmos Chem Phys, 12, 2567-2585, 10.5194/acp-12-2567-2012, 2012.

Levy, H.: Normal Atmosphere: Large Radical and Formaldehyde Concentrations Predicted, Science, 173,

https://doi.org/10.5194/egusphere-2024-2494
Preprint. Discussion started: 30 August 2024

141-143, 10.1126/science.173.3992.141, 1971.
Li, S., Lu, K., Ma, X., Yang, X., Chen, S., and Zhang, Y.: Field measurement of the organic peroxy radicals by the low-pressure reactor plus laser-induced fluorescence spectroscopy, Chinese Chemical Letters, 31, 2799-2802, 10.1016/j.cclet.2020.07.051, 2020.
Liu, S., Li, X., Shen, X., Zeng, L., Huang, X., Zhu, B., Lin, L., and Lou, S.: Measurement and partition analysis of atmospheric OH reactivity in autumn in Shenzhen, Acta Scientiae Circumstantiae, 39, 3600-3610, 2019.
Liu, Y., Li, J., Ma, Y., Zhou, M., Tan, Z., Zeng, L., Lu, K., and Zhang, Y.: A review of gas-phase chemical mechanisms commonly used in atmospheric chemistry modelling, Journal of Environmental Sciences, 10.1016/j.jes.2022.10.031, 2022.
Liu, Z., Wang, Y., Hu, B., Lu, K., Tang, G., Ji, D., Yang, X., Gao, W., Xie, Y., Liu, J., Yao, D., Yang, Y., and Zhang, Y.: Elucidating the quantitative characterization of atmospheric oxidation capacity in Beijing, China, Sci Total Environ, 771, 10.1016/j.scitotenv.2021.145306, 2021.
Lou, S., Holland, F., Rohrer, F., Lu, K., Bohn, B., Brauers, T., Chang, C. C., Fuchs, H., Haseler, R., Kita, K., Kondo, Y., Li, X., Shao, M., Zeng, L., Wahner, A., Zhang, Y., Wang, W., and Hofzumahaus, A.: Atmospheric OH reactivities in the Pearl River Delta – China in summer 2006: measurement and model results, Atmos Chem Phys, 10, 11243–11260, 10.5194/acp-10-11243-2010, 2010.
Lu, K. D., Guo, S., Tan, Z. F., Wang, H. C., Shang, D. J., Liu, Y. H., Li, X., Wu, Z. J., Hu, M., and Zhang, Y. H.: Exploring atmospheric free-radical chemistry in China: the self-cleansing capacity and the formation of secondary air pollution, Natl. Sci. Rev., 6, 579-594, 10.1093/nsr/nwy073, 2019.
Lu, K. D., Rohrer, F., Holland, F., Fuchs, H., Bohn, B., Brauers, T., Chang, C. C., Haeseler, R., Hu, M., Kita, K., Kondo, Y., Li, X., Lou, S. R., Nehr, S., Shao, M., Zeng, L. M., Wahner, A., Zhang, Y. H., and Hofzumahaus, A.: Observation and modelling of OH and HO_2 concentrations in the Pearl River Delta 2006: a missing OH source in a VOC rich atmosphere, Atmos Chem Phys, 12, 1541-1569, 10.5194/acp-12-1541-2012, 2012.
Ma, X., Tan, Z., Lu, K., Yang, X., Chen, X., Wang, H., Chen, S., Fang, X., Li, S., Li, X., Liu, J., Liu, Y., Lou, S., Qiu, W., Wang, H., Zeng, L., and Zhang, Y.: OH and HO_2 radical chemistry at a suburban site during the EXPLORE-YRD campaign in 2018, Atmos Chem Phys, 22, 7005-7028, 10.5194/acp-22-7005-2022, 2022.
Ma, X. F., Tan, Z. F., Lu, K. D., Yang, X. P., Liu, Y. H., Li, S. L., Li, X., Chen, S. Y., Novelli, A., Cho, C. M., Zeng, L. M., Wahner, A., and Zhang, Y. H.: Winter photochemistry in Beijing: Observation and model simulation of OH and HO_2 radicals at an urban site, Sci Total Environ, 685, 85-95, 10.1016/j.scitotenv.2019.05.329, 2019.
Mao, J., Ren, X., Chen, S., Brune, W. H., Chen, Z., Martinez, M., Harder, H., Lefer, B., Rappenglück, B., Flynn, J., and Leuchner, M.: Atmospheric oxidation capacity in the summer of Houston 2006: Comparison with summer measurements in other metropolitan studies, Atmos Environ, 44, 4107-4115, 10.1016/j.atmosenv.2009.01.013, 2010.
Martinez, M., Harder, H., Kovacs, T. A., Simpas, J. B., Bassis, J., Lesher, R., Brune, W. H., Frost, G. J., Williams, E. J., Stroud, C. A., Jobson, B. T., Roberts, J. M., Hall, S. R., Shetter, R. E., Wert, B., Fried, A., Alicke, B., Stutz, J., Young, V. L., White, A. B., and Zamora, R. J.: OH and HO_2 concentrations, sources, and loss rates during the Southern Oxidants Study in Nashville, Tennessee, summer 1999, J Geophys Res-Atmos, 108, 10.1029/2003jd003551, 2003.
Peeters, J., Muller, J. F., Stavrakou, T., and Nguyen, V. S.: Hydroxyl Radical Recycling in Isoprene Oxidation Driven by Hydrogen Bonding and Hydrogen Tunneling: The Upgraded LIM1 Mechanism, J Phys Chem A, 118, 8625-8643, 10.1021/jp5033146, 2014.
Qu, H., Wang, Y., Zhang, R., Liu, X., Huey, L. G., Sjostedt, S., Zeng, L., Lu, K., Wu, Y., Shao, M., Hu, M., Tan, Z., Fuchs, H., Broch, S., Wahner, A., Zhu, T., and Zhang, Y.: Chemical Production of Oxygenated Volatile Organic Compounds Strongly Enhances Boundary-Layer Oxidation Chemistry and Ozone Production, Environ Sci Technol, 10.1021/acs.est.1c04489, 2021.
Ren, X., Olson, J. R., Crawford, J. H., Brune, W. H., Mao, J., Long, R. B., Chen, Z., Chen, G., Avery, M. A., Sachse, G. W., Barrick, J. D., Diskin, G. S., Huey, L. G., Fried, A., Cohen, R. C., Heikes, B., Wennberg, P. O., Singh, H. B., Blake, D. R., and Shetter, R. E.: HOx chemistry during INTEX-A 2004: Observation, model calculation, and comparison with previous studies, J Geophys Res-Atmos, 113, 10.1029/2007jd009166, 2008.
Rohrer, F., Lu, K., Hofzumahaus, A., Bohn, B., Brauers, T., Chang, C.-C., Fuchs, H., Haeseler, R., Holland, F., Hu, M., Kita, K., Kondo, Y., Li, X., Lou, S., Oebel, A., Shao, M., Zeng, L., Zhu, T., Zhang, Y., and

https://doi.org/10.5194/egusphere-2024-2494
Preprint. Discussion started: 30 August 2024

Wahner, A.: Maximum efficiency in the hydroxyl-radical-based self-cleansing of the troposphere, Nature Geoscience, 7, 559-563, 10.1038/ngeo2199, 2014.
Shi, X., Ge, Y., Zheng, J., Ma, Y., Ren, X., and Zhang, Y.: Budget of nitrous acid and its impacts on atmospheric oxidative capacity at an urban site in the central Yangtze River Delta region of China, Atmos Environ, 238, 10.1016/j.atmosenv.2020.117725, 2020.
Shirley, T. R., Brune, W. H., Ren, X., Mao, J., Lesher, R., Cardenas, B., Volkamer, R., Molina, L. T., Molina, M. J., Lamb, B., Velasco, E., Jobson, T., and Alexander, M.: Atmospheric oxidation in the Mexico City Metropolitan Area (MCMA) during April 2003, Atmos Chem Phys, 6, 2753-2765, 10.5194/acp-6-2753-2006, 2006.
Slater, E. J., Whalley, L. K., Woodward-Massey, R., Ye, C., Lee, J. D., Squires, F., Hopkins, J. R., Dunmore, R. E., Shaw, M., Hamilton, J. F., Lewis, A. C., Crilley, L. R., Kramer, L., Bloss, W., Vu, T., Sun, Y., Xu, W., Yue, S., Ren, L., Acton, W. J. F., Hewitt, C. N., Wang, X., Fu, P., and Heard, D. E.: Elevated levels of OH observed in haze events during wintertime in central Beijing, Atmos Chem Phys, 20, 14847-14871, 10.5194/acp-20-14847-2020, 2020.
Stockwell, W. R., Kirchner, F., Kuhn, M., and Seefeld, S.: A new mechanism for regional atmospheric chemistry modeling, J Geophys Res-Atmos, 102, 25847-25879, 10.1029/97jd00849, 1997.
Stone, D., Whalley, L. K., and Heard, D. E.: Tropospheric OH and HO_2 radicals: field measurements and model comparisons, Chemical Society reviews, 41, 6348-6404, 10.1039/c2cs35140d, 2012.
Tan, Z., Ma, X., Lu, K., Jiang, M., Zou, Q., Wang, H., Zeng, L., and Zhang, Y.: Direct evidence of local photochemical production driven ozone episode in Beijing: A case study, Sci Total Environ, 800, 148868, 10.1016/j.scitotenv.2021.148868, 2021.
Tan, Z., Lu, K., Jiang, M., Su, R., Wang, H., Lou, S., Fu, Q., Zhai, C., Tan, Q., Yue, D., Chen, D., Wang, Z., Xie, S., Zeng, L., and Zhang, Y.: Daytime atmospheric oxidation capacity in four Chinese megacities during the photochemically polluted season: a case study based on box model simulation, Atmos Chem Phys, 19, 3493-3513, 10.5194/acp-19-3493-2019, 2019.
Tan, Z., Fuchs, H., Lu, K., Hofzumahaus, A., Bohn, B., Broch, S., Dong, H., Gomm, S., Haeseler, R., He, L., Holland, F., Li, X., Liu, Y., Lu, S., Rohrer, F., Shao, M., Wang, B., Wang, M., Wu, Y., Zeng, L., Zhang, Y., Wahner, A., and Zhang, Y.: Radical chemistry at a rural site (Wangdu) in the North China Plain: observation and model calculations of OH, HO_2 and RO_2 radicals, Atmos Chem Phys, 17, 663-690, 10.5194/acp-17-663-2017, 2017a.
Tan, Z. F., Lu, K. D., Dong, H. B., Hu, M., Li, X., Liu, Y. H., Lu, S. H., Shao, M., Su, R., Wang, H. C., Wu, Y. S., Wahner, A., and Zhang, Y. H.: Explicit diagnosis of the local ozone production rate and the ozone-NOx-VOC sensitivities, Sci. Bull., 63, 1067-1076, 10.1016/j.scib.2018.07.001, 2018.
Tan, Z. F., Fuchs, H., Lu, K. D., Hofzumahaus, A., Bohn, B., Broch, S., Dong, H. B., Gomm, S., Haseler, R., He, L. Y., Holland, F., Li, X., Liu, Y., Lu, S. H., Rohrer, F., Shao, M., Wang, B. L., Wang, M., Wu, Y. S., Zeng, L. M., Zhang, Y. S., Wahner, A., and Zhang, Y. H.: Radical chemistry at a rural site (Wangdu) in the North China Plain: observation and model calculations of OH, HO_2 and RO_2 radicals, Atmos Chem Phys, 17, 663-690, 10.5194/acp-17-663-2017, 2017b.
Wang, F., Hu, R., Xie, P., Wang, Y., Chen, H., Zhang, G., and Liu, W.: Calibration source for OH radical based on synchronous photolysis, Acta Phys Sin-Ch Ed, 69, 2020.
Wang, F. Y., Hu, R. Z., Chen, H., Xie, P. H., Wang, Y. H., Li, Z. Y., Jin, H. W., Liu, J. G., and Liu, W. Q.: Development of a field system for measurement of tropospheric OH radical using laser-induced fluorescence technique, Opt. Express, 27, A419-A435, 10.1364/oe.27.00a419, 2019a.
Wang, H., Lu, K., Tan, Z., Chen, X., Liu, Y., and Zhang, Y.: Formation mechanism and control strategy for particulate nitrate in China, Journal of Environmental Sciences, 10.1016/j.jes.2022.09.019, 2022a.
Wang, H., Ma, X., Tan, Z., Wang, H., Chen, X., Chen, S., Gao, Y., Liu, Y., Liu, Y., Yang, X., Yuan, B., Zeng, L., Huang, C., Lu, K., and Zhang, Y.: Anthropogenic monoterpenes aggravating ozone pollution, Natl. Sci. Rev., 9, 2022b.
Wang, S.-n., Wu, R.-r., and Wang, L.-m.: Role of hydrogen migrations in carbonyl peroxy radicals in the atmosphere, Chinese J Chem Phys, 32, 457-466, 10.1063/1674-0068/cjcp1811265, 2019b.
Wang, T., Xue, L., Feng, Z., Dai, J., Zhang, Y., and Tan, Y.: Ground-level ozone pollution in China: a synthesis of recent findings on influencing factors and impacts, Environmental Research Letters, 10.1088/1748-9326/ac69fe, 2022c.
Wang, Y., Hu, R., Xie, P., Chen, H., Wang, F., Liu, X., Liu, J., and Liu, W.: Measurement of tropospheric HO_2 radical using fluorescence assay by gas expansion with low interferences, J Environ Sci (China), 99, 40-50, 10.1016/j.jes.2020.06.010, 2021.

https://doi.org/10.5194/egusphere-2024-2494
Preprint. Discussion started: 30 August 2024

Whalley, L. K., Blitz, M. A., Desservettaz, M., Seakins, P. W., and Heard, D. E.: Reporting the sensitivity of laser-induced fluorescence instruments used for HO_2 detection to an interference from RO_2 radicals and introducing a novel approach that enables HO_2 and certain RO_2 types to be selectively measured, Atmos Meas Tech, 6, 3425-3440, 10.5194/amt-6-3425-2013, 2013.

Whalley, L. K., Stone, D., Dunmore, R., Hamilton, J., Hopkins, J. R., Lee, J. D., Lewis, A. C., Williams, P., Kleffmann, J., Laufs, S., Woodward-Massey, R., and Heard, D. E.: Understanding in situ ozone production in the summertime through radical observations and modelling studies during the Clean air for London project (ClearfLo), Atmos Chem Phys, 18, 2547-2571, 10.5194/acp-18-2547-2018, 2018.

Whalley, L. K., Slater, E. J., Woodward-Massey, R., Ye, C., Lee, J. D., Squires, F., Hopkins, J. R., Dunmore, R. E., Shaw, M., Hamilton, J. F., Lewis, A. C., Mehra, A., Worrall, S. D., Bacak, A., Bannan, T. J., Coe, H., Percival, C. J., Ouyang, B., Jones, R. L., Crilley, L. R., Kramer, L. J., Bloss, W. J., Vu, T., Kotthaus, S., Grimmond, S., Sun, Y., Xu, W., Yue, S., Ren, L., Acton, W. J. F., Hewitt, C. N., Wang, X., Fu, P., and Heard, D. E.: Evaluating the sensitivity of radical chemistry and ozone formation to ambient VOCs and NOx in Beijing, Atmos Chem Phys, 21, 2125-2147, 10.5194/acp-21-2125-2021, 2021.

Woodward-Massey, R., Sommariva, R., Whalley, L. K., Cryer, D. R., Ingham, T., Bloss, W. J., Ball, S. M., Cox, S., Lee, J. D., Reed, C. P., Crilley, L. R., Kramer, L. J., Bandy, B. J., Forster, G. L., Reeves, C. E., Monks, P. S., and Heard, D. E.: Radical chemistry and ozone production at a UK coastal receptor site, Atmos Chem Phys, 23, 14393-14424, 10.5194/acp-23-14393-2023, 2023.

Yang, X., Lu, K., Ma, X., Gao, Y., Tan, Z., Wang, H., Chen, X., Li, X., Huang, X., He, L., Tang, M., Zhu, B., Chen, S., Dong, H., Zeng, L., and Zhang, Y.: Radical chemistry in the Pearl River Delta: observations and modeling of OH and HO_2 radicals in Shenzhen in 2018, Atmos Chem Phys, 22, 12525-12542, 10.5194/acp-22-12525-2022, 2022.

Yang, X., Lu, K., Ma, X., Liu, Y., Wang, H., Hu, R., Li, X., Lou, S., Chen, S., Dong, H., Wang, F., Wang, Y., Zhang, G., Li, S., Yang, S., Yang, Y., Kuang, C., Tan, Z., Chen, X., Qiu, P., Zeng, L., Xie, P., and Zhang, Y.: Observations and modeling of OH and HO_2 radicals in Chengdu, China in summer 2019, The Science of the total environment, 772, 144829-144829, 10.1016/j.scitotenv.2020.144829, 2021a.

Yang, Y., Li, X., Zu, K., Lian, C., Chen, S., Dong, H., Feng, M., Liu, H., Liu, J., Lu, K., Lu, S., Ma, X., Song, D., Wang, W., Yang, S., Yang, X., Yu, X., Zhu, Y., Zeng, L., Tan, Q., and Zhang, Y.: Elucidating the effect of HONO on O_3 pollution by a case study in southwest China, Sci Total Environ, 756, 144127, 10.1016/j.scitotenv.2020.144127, 2021b.

Yugo Kanaya, Renqiu Cao, Hajime Akimoto, Masato Fukuda, Yuichi Komazaki, Yoko Yokouchi, Makoto Koike, Hiroshi Tanimoto, Nobuyuki Takegawa, and Kondo, a. Y.: Urban photochemistry in central Tokyo: 1. Observed and modeled OH and HO_2 radical concentrations during the winter and summer of 2004, J Geophys Res-Atmos, 112, 20, 10.1029/2007JD008670, 2007.

Yugo Kanaya, R. C., Shungo Kato, Yuko Miyakawa, Yoshizumi Kajii, Hiroshi and Tanimoto, Y. Y., Michihiro Mochida, Kimitaka Kawamura, Hajime Akimoto: Chemistry of OH and HO_2 radicals observed at Rishiri Island, Japan, in September 2003: Missing daytime sink of HO_2 and positive nighttime correlations with monoterpenes, J Geophys Res-Atmos, 112, 10.1029/2006id007987, 2007.

Zhang, G., Hu, R., Xie, P., Lou, S., Wang, F., Wang, Y., Qin, M., Li, X., Liu, X., Wang, Y., and Liu, W.: Observation and simulation of HOx radicals in an urban area in Shanghai, China, Sci Total Environ, 810, 152275, 10.1016/j.scitotenv.2021.152275, 2022a.

Zhang, G., Hu, R., Xie, P., Lu, K., Lou, S., Liu, X., Li, X., Wang, F., Wang, Y., Yang, X., Cai, H., Wang, Y., and Liu, W.: Intercomparison of OH radical measurement in a complex atmosphere in Chengdu, China, Sci Total Environ, 155924, 10.1016/j.scitotenv.2022.155924, 2022b.